# Section 4

# Parameterization of important atmospheric and surface processes, effects of different parameterizations

# Dependency of horizontal resolution and turbulent scheme on accumulation processes of low-level water vapor

Teruyuki KATO

Meteorological Research Institute, Tsukuba, Ibaraki, Japan (E-mail: tkato@mri-jma.go.jp)

## 1. Introduction

On 6 May, 2012, a supercell storm caused a strong tornado with Fujita scale 3 that struck Tsukuba City, located Kanto Plain in the middle part of Japan. The major formation factor of the supercell was the inflow of low-level humid air from the Pacific Ocean, as well as large temperature difference in the vertical (Kato 2013). In this study, the dependency of horizontal resolution and turbulent scheme on accumulation processes of low-level water over the ocean is examined using the Japan Meteorological Agency (JMA) nonhydrostatic model (Saito et al. 2007).

## 2. Experimental designs

Twelve-hour forecasts from 18 JST (=UTC+ 9hours) 05 May 2012 are conducted using initial and boundary conditions produced from 3-hourly available JMA mesoscale analyses with a horizontal resolution of 5 km. At first a 5km-resolution simulation with a large domain (2500x2000km) was conducted, and then the other simulations with a small domain (1000x600km) are conducted directly nested within large-domain forecasts. Horizontal resolutions of 5km, 2km, 1km and 500m are used, and 50 stretched layers (6 of which are set below a height of 500 m) are set in the vertical. A bulk-type microphysics parameterization scheme in which two moments are treated only for ice hydrometeors is used for precipitation processes, and the Kain- Fritsch convection parameterization scheme is additionally used only in 5km models. The turbulence closure scheme of Mellor-Yamada-Nakanishi-Niino level-3 (MYNN, Nakanishi and Niino 2006) is used in 5km, 2km, and 1km models, while Deardorff scheme (DD, 1980) is used in 1km and 500m models. Surface fluxes are calculated by a bulk method, in which the bulk coefficients are determined from the formula of Berjaars and Holtslag (1991) over both the sea and land.

## 3. Accumulation processes of low-level water vapor

In order to examine accumulation processes of low-level water, a budget analysis is made for water vapor amounts in vertical columns below a height of 936m (LWA). Local time difference of LWA is described as

$$\frac{\partial \mathrm{LWP}}{\partial t} = \mathrm{Conv_h} + \mathrm{Adv_v} + \mathrm{LH} + \mathrm{Others}, \quad (1)$$

where $\mathrm{Conv_h}$ is the horizontal convergence from lateral boundaries, $\mathrm{Adv_v}$ is the vertical transportation at upper panels of the vertical columns, LH is the latent heat flux from the surface, and Others denote the changes through condensation and evaporation. The last term is negligible because no cloud was found over the analysis domain.

An area with LWA ~ 8 mm on the left side of Fig. 1 at the initial (hereafter, called as target air column) moves east-northeastward, and after 12 hours the value of LWA increases by about 3 mm. A significant increase is found during the period when the air column crossed over a region with high sea surface temperature. A budget of the LWA in the target air column is examined.

The residual in the target air column calculated from $\mathrm{Conv_h}$ and $\mathrm{Adv_v}$ is considerably larger than the increase from LH, and total local change (RHS in Eq. (1)) is larger than the Lagrangian change directly calculated from LWA (Fig. 2a). This is caused by no consideration of horizontal advection ($\mathrm{Adv_h}$) as follows.

$$\frac{\mathrm{dLWP}}{\mathrm{dx}} = \frac{\partial \mathrm{LWP}}{\partial t} + \mathrm{Adv_h} \quad (2)$$

Here, $\mathrm{Adv_h}$ is estimated using winds at a height of 844m. Red lines in Fig. 2a show that the Lagrangian change calculated from Eqs. (1) and (2) almost agrees with the direct calculation from LWA, indicating the budget analysis is successful.

The kinematic change of LWA defined by the sum of $\mathrm{Conv_h}$ , $\mathrm{Adv_v}$ and $\mathrm{Adv_h}$ is compared with the increase amount from LH (Fig. 2b). About two third of LWA increase (~ 2mm) is brought from the kinematic change, while the remaining is from LH. The increase over the ocean with high temperature is mainly from LH, while the kinematic change is dominant after 6 hour forecast.

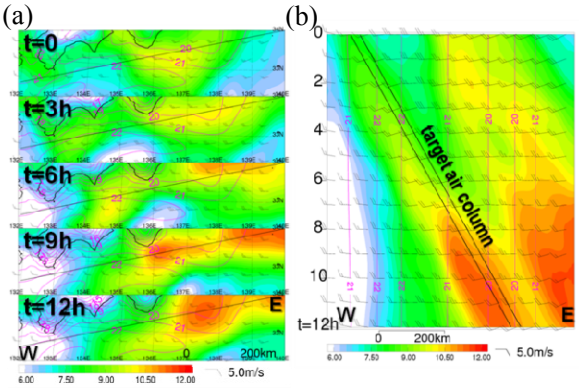


Fig. 1 (a) Distributions of 5km-model simulated LWA from the initial to 12 h forecast and (b) Hovmoller diagram across black lines in (a). Arrows show 936m- height horizontal winds, and pink contours show distributions of sea surface temperature.

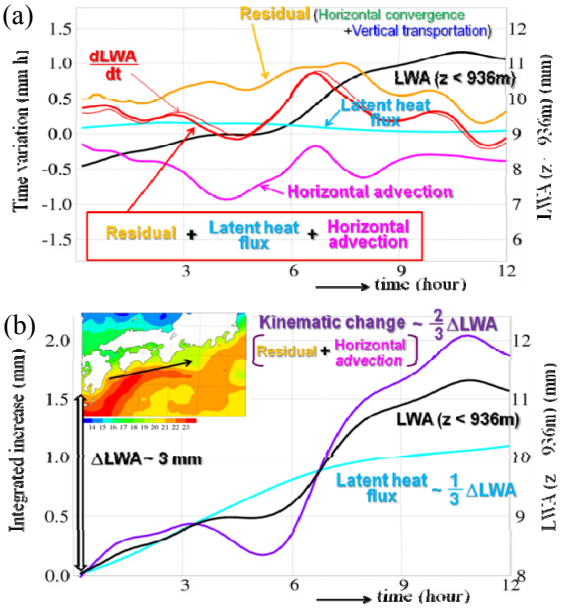


Fig. 2 (a) Time changes of 5km-model simulated LWA and its budgets for the target column shown in Fig. 1b and (b) those of integrated increases in kinematic change and latent heat flux. Thin red line in (a) shows the change directly calculated from LWA. Left-top panel in (b) shows the distribution of SST.

## 3. Dependency of horizontal resolution and turbulent scheme

Table 1 shows the contributions of kinematic change and LH on accumulation processes of low-level water for different horizontal resolutions and turbulent schemes of numerical models. The dependency on total increase is small; however, the contributions of kinematic change and LH are different for turbulent schemes. LH is smaller for DD, while the kinematic change is larger. It should be noted that the difference for horizontal resolution is remarkably smaller than that for turbulent schemes.

The above-mentioned differences are examined from water vapor amounts that are vertically transported by sub-grid and grid-resolved vertical motions (Fig. 3). Sub-grid transportation is almost limited below a height of 500m that is lower for DD. MYNN transports more water vapor upward than DD, which causes the difference in LH. Grid-resolved motions also transport more water vapor for MYNN, especially above a height of 500m, which reduces the accumulation amounts in the kinematic change.

Table 1 Total increases for the target air column, accumulated for 12 hours and their contents (kinematic change and latent heat flux).

| | 500m(DD) | | 1km(DD) | |
|---|---|---|---|---|
| Total (mm/12hours) | 2.85 | - | 2.93 | - |
| Kinematic change | 2.11 | 74.3% | 2.21 | 75.5% |
| Latent heat flux | 0.73 | 25.7% | 0.72 | 24.5% |
| **5km(MYNN)** | | **2km(MYNN)** | | **1km(MYNN)** |
| 3.06 | - | 2.78 | - | 2.87 | - |
| 1.97 | 64.2% | 1.71 | 61.4% | 1.80 | 62.9% |
| 1.10 | 35.8% | 1.07 | 38.5% | 1.06 | 37.1% |

Last, vertical profiles of water vapor for the target air column are compared (Fig. 4). The increase of water vapor amounts near the surface for MYNN is almost a half for DD because of larger sub-grid transportation of water vapor. The difference between MYNN and DD is about 1 g/kg below a height of 400m. Meanwhile, water vapor is more accumulated for MYNN above a height of 500m. The difference for horizontal resolutions is also smaller than that for turbulent schemes. These results indicate that moist convection more easily forms using DD than using MYNN, although almost the same LWA is accumulated.

## References


Beljaars, A.C.M. and A.A.M. Holtslag, 1991: *J. Appl. Meteor.*, **30**, 327-341.

Deardorff, J. W., 1980: *Bound.-Layer. Meteorol.*, **18**, 495-527.

Kato, 2013: *CAS/JSC Research Activities in Atmospheric and Oceanic Modeling*, **43**, 5.07-5.08.

Nakanishi, M. and H. Niino, 2006: *Bound.-Layer Meteor.*, **119**, 397- 407.

Saito, K., et al., 2007: *J. Meteor. Soc. Japan*, **85B**, 271-304.


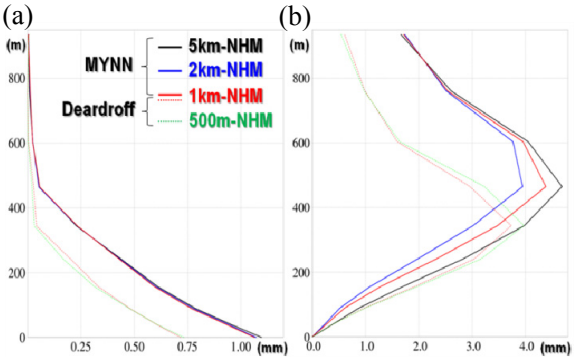


Fig.3 Vertical profiles of vertical transportation amounts of water vapor for the target air column, accumulated for 12 hours, by (a) sub-grid and (b) grid-resolved vertical motions.

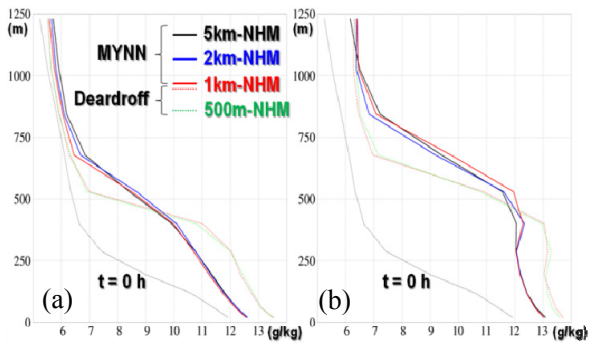


Fig. 4 Vertical profiles of water vapor for the target air column at (a) t = 6 hours and (b) t = 12 hours. The profile at the initial time is also drawn in each panel.

# Evaluating aerosol impacts on Numerical Weather Prediction in an extreme dust event

S. Remy, A. Benedetti, L. Jones, M. Razinger and T. Haiden

European Centre for Medium-Range Weather Forecasts, Reading, UK.,
samuel.remy@ecmwf.int

The WMO-sponsored Working Group on Numerical Experimentation (WGNE) set up a project aimed at understanding the importance of aerosols for numerical weather prediction (NWP). Three cases are being investigated by several NWP centres with aerosol capabilities: a severe dust case that affected the Eastern Mediterranean in April 2012, a biomass burning case in South America in September 2012, and an extreme pollution event in Beijing in January 2013. At ECMWF these cases were studied using the MACC-II system with radiatively interactive aerosols. Here we focus on the dust case and discuss the feedback between dust aerosols and boundary layer meteorology caused by the aerosol direct effect. As there was no cloud in this situation, the aerosol indirect effect is of no significance here.

The dust storm that affected Libya, Egypt and the middle East from 17th to 19th of April 2012 was caused by a heat low crossing Libya from Southwest to Northeast; it brought some very high dust aerosol concentrations, with Aerosol Optical Depth (AOD) at 550nm reaching a value above four at Cairo late on 18th of April 2012. The dust aerosol direct radiative forcing had a strong impact on both the shortwave down-welling radiation at surface, which was reduced by 20 to 30% and on long-wave downward radiation, which was increased by 30 to 40%. Comparison of forecasted and observed radiation at Tamanrasset (Algeria) for this event showed that forecasts were generally more accurate when taking into account the aerosol direct effect, both in the shortwave and in the long-wave spectra.

As the concerned areas are of desert type, i.e. with a sandy soil that favours strong night-time cooling, the aerosol layer radiative forcing in the long-wave spectrum, acting in a similar way as a cloud layer, had locally a large warming effect during the night : up to 4-5 K at places. This is clearly shown in Figure 1, which shows temperature, AOD and long-wave radiation at Asyut (Egypt). The minimum temperatures forecasted with experiments taking into account the aerosol direct effect were generally closer to observations for a wide range of stations in Egypt, Libya and Israel.

The impact of reduced shortwave radiation on maximum temperatures was much smaller; it was probably overshadowed by the higher night-time temperatures. Daytime warming brought by shortwave radiation was smaller when taking into account the aerosol direct effect; both because around 20% of incoming solar radiation was absorbed by the aerosol layer and because the night-time temperatures were higher.

Because of higher night-time temperatures, the lower atmosphere was less stable at night and the heat low that was at the origin of the dust storm was deeper. This in turn increased the strength of the winds over the desert. With more effective saltation processes, which are modelled as a function of 10m wind speed to the cubic power, dust aerosol sources were also significantly increased. As a consequence, dust AOD was around 20% higher during the storm when taking into account the aerosol direct effect, as shown by Figure 1. The forecasted AOD peak during the storm, which was underestimated, was brought closer to observations.

This study revealed a positive feedback between dust aerosols and boundary layer meteorology during an extreme dust aerosol event. It was already well known that aerosols impacts low and middle troposphere through the direct and indirect effect; however the fact that these modifications on boundary layer meteorology affect in turn the aerosol load appears not to have been documented yet.

**References:**


Benedetti, A., Morcrette, J.-J., Boucher, O., Dethof, A., Engelen,R. J., Fisher, M., Flentje, H., Huneeus, N., Jones, L., Kaiser,J. W., Kinne, S., Manglold, A., Razinger, M., Simmons, A. J.,and Suttie, M.: Aerosol analysis and forecast in the European Centre for Medium-Range Weather Forecasts Integrated Forecast System: 2. Data assimilation, J. Geophys. Res., 114, D13205. 2009.

Morcrette, J.-J., Boucher, O., Jones, L., Salmond, D., Bechtold, P., Beljaars, A., Benedetti, A., Bonet, A., Kaiser, J. W., Razinger, M., Schulz, M., Serrar, S., Simmons, A. J., Sofiev, M., Suttie, M., Tompkins, A. M., and Untch, A.: Aerosol analysis and forecast in the European Centre for Medium-Range Weather Forecasts Integrated Forecast System: Forward modeling, J. Geophys. Res., 114, D06206, 2009.


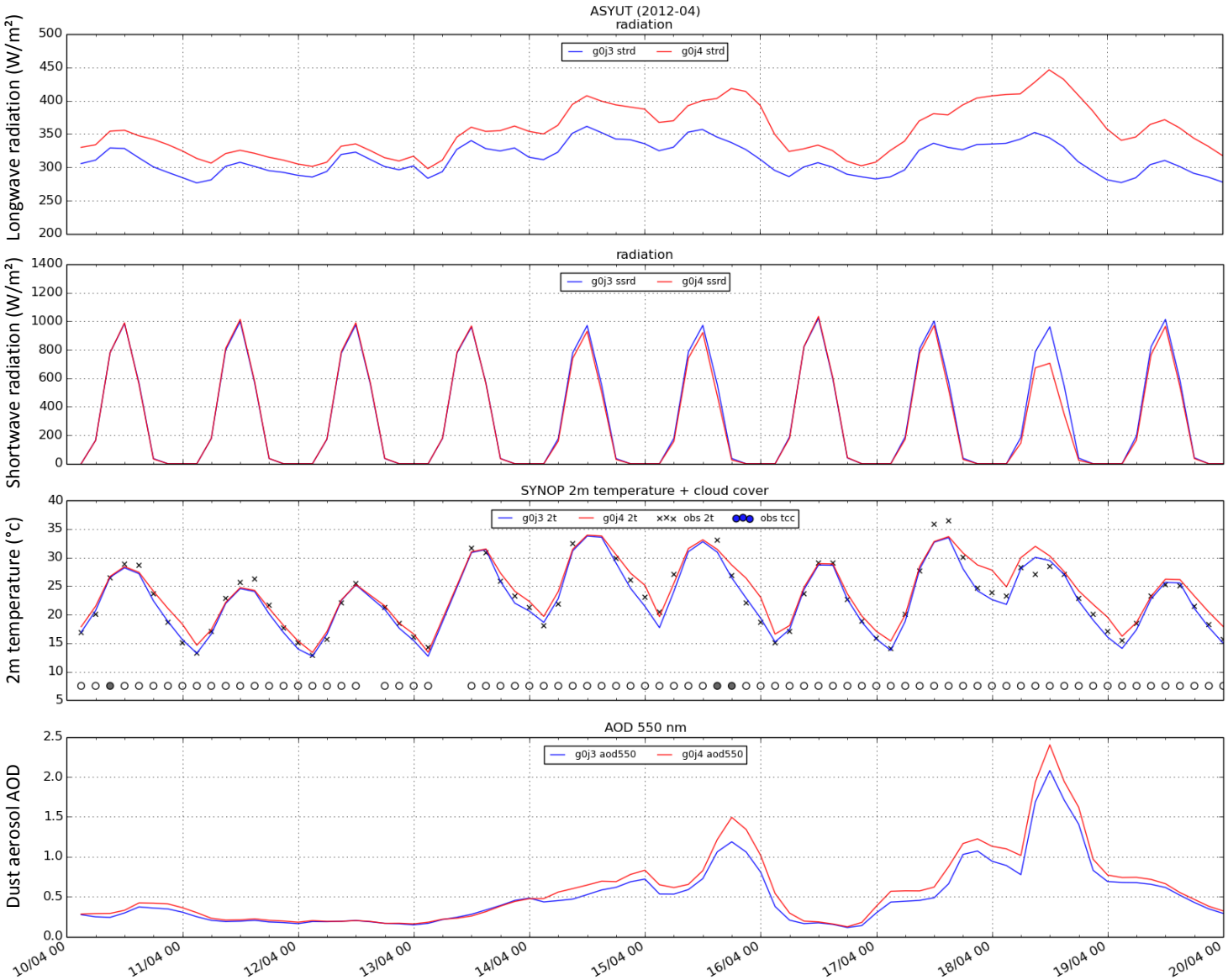


*Figure 1: forecasts with (red) and without (blue) taking into account the aerosol direct effect, at Asyut (Egypt), from 10th to 20th of April 2012. Forecasts starting at 0UTC everyday, 3-24h forecast times. From top to bottom: downward longwave radiation at surface, downward shortwave radiation at surface, 2m temperature and dust aerosol AOD at 550nm. Observations of 2m temperature are also indicated with black crosses, together with cloud cover.*

# Urban impact on summertime precipitation in Tokyo: Numerical simulation using NHM and the Square Prism Urban Canopy scheme

Naoko Seino, Toshinori Aoyagi, and Hiroshige Tsuguti
*Meteorological Research Institute, Japan Meteorological Agency, 1-1, Nagamine, Tsukuba 305-0052, Japan*
E-mail: nseino@mri-jma.go.jp

## 1. Background

Precipitation modification due to increasing urbanization is one of the key topics in the urban climate research. Recently, Fujibe et al. (2009) showed that precipitation amounts observed in central Tokyo had statistically significant increasing trend and positive spatial anomaly to those in surrounding areas in the afternoon of warm season. However, the detected change in precipitation can be influenced by factors other than urbanization, such as global warming and associated regional climate change. For the better understanding of urban impact on precipitation, numerical modeling with a high-performance urban scheme is a useful approach. In the present research, numerical simulations for August in recent eight years have been conducted to investigate how increasing heat island intensity in Tokyo affects precipitation in the metropolitan area and its vicinities.

## 2. Experimental design

The Non-hydrostatic Model (NHM) of Japan Meteorological Agency (JMA) is utilized in the simulations (Saito et al., 2007). Horizontal grid interval is 2km and the model domain covers central Japan including Tokyo metropolitan area (Fig. 1). The Square Prism Urban Canopy (SPUC) scheme (Aoyagi and Seino, 2011) is incorporated in NHM. SPUC is a kind of single-layer urban canopy scheme. In contrast to the slab land surface scheme used in the operational version of NHM, SPUC takes into account heat and radiation exchanges by urban canopy elements in the surface heat budget. Spatial distribution of time-varying anthropogenic heat in the metropolitan area (Senoo et al., 2004) is also considered in SPUC. Area fractions of buildings and other land use categories in each model grid are determined from the 100m-mesh Digital National Land Information Dataset.

Comparative experiments have been done with and without SPUC for August from 2006 to 2013. In the SPUC experiment, SPUC scheme is applied in highly urbanized grids mainly in the central Tokyo area where area fraction of building lots is higher than 80%. On the other hand, in the SLAB experiment, slab land surface treatment is applied in the entire domain with urban surface parameters representing moderate urban conditions. Time integrations for 27 hours starting at 21 JST (Japan Standard Time, UTC+9hr) are repeated in both experiments. Initial and boundary conditions are given from operational mesoscale analyses of JMA. Simulation results in the two experiments from forecast time FT=3 to FT=27 (from 00 to 24 JST) are compared.

## 3. Results

Difference in the monthly mean surface temperature between the SPUC and SLAB experiments is shown in Fig. 1; simulated mean surface temperature of the SPUC experiment was higher up to 0.8K in the area where the surface scheme is changed. At Ohtemachi (business district) and Nerima (residential area) both located in Tokyo, simulated temperatures in the SPUC experiment were higher especially in the night-time, which agreed in general with observations (figure not shown). This indicates that realistic temperature field was simulated in the SPUC experiment in both diurnal temperature variation and heat island intensity.

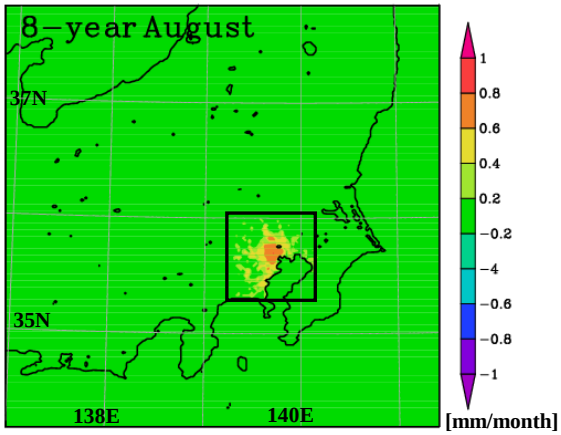


Fig. 1 Model domain and simulated 8-year August surface temperature difference between the SPUC and SLAB experiments. A rectangle indicates the reference urban area.

Monthly precipitation amounts were reasonably well simulated in both the SPUC and SLAB experiments. Difference in monthly precipitation between the experiments (SPUC-SLAB) is shown in Fig.2. Changes in rainfall distribution appear scattered in a wide area compared to the reference area where the urban surface scheme is replaced. We can also see that the precipitation increase is often coupled with its decrease nearby. Thus we evaluated area-averaged precipitation amounts in several rectangles with (k*10 + 1) km length (k=1-11) of each side, centered at the most urbanized area.

A larger amount of monthly precipitation in the SPUC experiment was found in domains with k ≦6 for the 8-year August mean. In domain 1, the most highly urbanized area, monthly precipitation amount was more than 10% larger in the SPUC experiment than in the SLAB experiment (Fig. 3). The normalized precipitation difference between the experiments decreases as the domain size increases. The differences were statistically significant by one-sided t-test at a significance level of 95% for domains 2 – 6, and 90% for domain 1.

Next, we examined daily maximum precipitation amount defined as the maximum value of the simulated daily precipitation among the grids in the domain every day. Figure 4 shows the scatter diagram of daily maximum precipitation in the SPUC and SLAB experiments in the reference urban area (domain 4). The linear regression line indicates that the SPUC experiment gives larger daily maximum precipitation amounts in domain 4 as well as the monthly precipitation amounts. It should be noted that the difference between the experiments were remarkable in some limited number of cases.

The present simulation results suggest that the temperature increase less than 1 °C in Tokyo area is likely to cause slight increase in summertime precipitation amounts in and around the area. However, differences in daily precipitation amounts and spatial distribution between the SPUC and SLAB experiments largely varied case by case. To examine the differences in more detail and obtain sufficiently meaningful features, additional simulations should be further conducted.

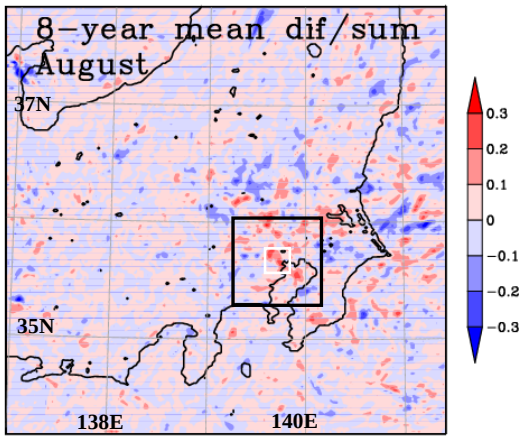


Fig. 2 Difference in monthly precipitation between SPUC and SLAB, defines as (SPUC-SLAB)/(0.5*(SPUC+SLAB)). A black rectangle indicates reference urban area (domain 4) and a white rectangle domain 1.

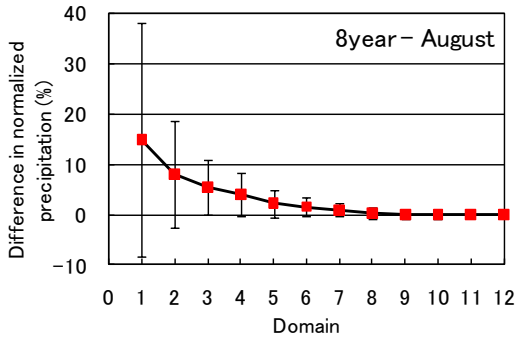


Fig. 3 Difference in normalized monthly precipitation between the SPUC and SLAB experiments (8-year August mean). Error bars denote standard deviations for 8 years.

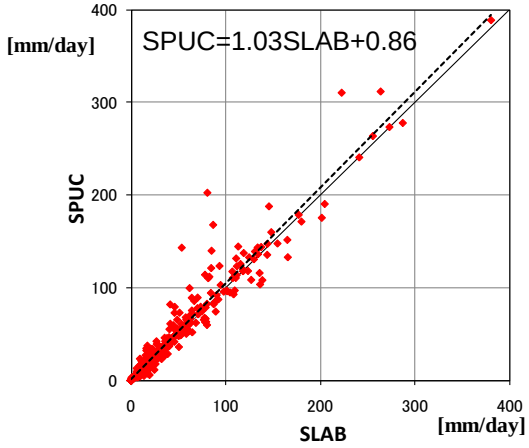


Fig. 4 Daily maximum precipitation amounts of the SPUC and SLAB experiments in the reference urban area (domain 4).

## References


Aoyagi, T. and N. Seino, (2011). A square prism urban canopy scheme for the NHM and its evaluation on summer conditions in the Tokyo metropolitan area, Japan. *J. Appl. Meteorol .Climatol.*, **50**, 1476-1496.

Fujibe, F., H. Togawa, and M. Sakata, (2009). Long-term change and spatial anomaly of warm season afternoon precipitation in Tokyo. *SOLA*, **5**, 17-20.

Saito, K., J. Ishida, K. Aranami, T. Hara, T. Segawa, M. Narita, and Y. Honda, 2007: Nonhydrostatic atmospheric models and operational development at JMA. *J. Meteor. Soc. Japan*, **85B**, 271-304.

Senoo, H., M. Kanda, T. Kinouchi, and A.Hagishima, (2004). Estimation of anthropogenic heat and vapour emission, and the impact on local meteorology. *Ann. J. Hydr. Eng.*, **48**, 160-174 (in Japanese with English abstract).

# New parameterizations of ice-phase processes in 3-ice bulk microphysical model

Yoshinori Yamada
Meteorological Research Institute, 1-1, Nagamine, Tsukuba, 305-0052, Japan
E-mail: yyamada@mri-jma.go.jp

## 1. Introduction

Ice-phase processes in the 3-ice bulk microphysical model (Ikawa and Saito 1991; Murakami 1990) integrated in the non-hydrostatic model of the Japan Meteorological Agency (hereafter JMA-NHM: e.g., Saito et al. 2006) have been used for a long time without substantial updates. Recent developments in bulk microphysical models (e.g., Ferrier 1994; Harrington et al. 1995; Morrison and Grabowski 2008), however, urge to improve the bulk models for better representation of clouds and precipitation. High performance bulk microphysical models are still indispensable because bulk models are widely used in numerical studies. This report describes some improvements in ice-phase processes in the 3-ice bulk microphysical model of JMA-NHM and preliminary results.

## 2. Outline of the new parameterizations of ice-processes

Improvements were mainly involved in cloud ice, snow, and graupel formation processes. These will be separately described below.

*a. Cloud ice process*

The size distribution of cloud ice is assumed to be an inverse-exponential type as for the snow and graupel. This assumption differs greatly from the mono-disperse assumption in the current model. The aggregation among cloud ice is computed by the strict solution (e.g., Verlinde et al. 1990) using temperature-dependent collection efficiency. The depositional growth of clod ice and the conversion from cloud ice to snow are modeled following the work of Harrington et al. (1995). Cloud ice whose diameter exceeding a prescribed value (set equal to 120$\mu$m in this study) is converted snow category. An excellence of this conversion lies in that only the portion of cloud ice of large size is transfered to snow unlike the current autoconversion which does not take into account the size of cloud ice particles. In this conversion calculation, an accurate and fast code for the calculation of incomplete Gamma function is employed.

*b. Aggregation of snow*

The current model of snow aggregation parameterization by Passarelli (1978) is substituted for the strict solution as for cloud ice. The temperature-dependent collection efficiency is also employed. A lower bound of the slope of the snow size distribution is imposed in order to implicitly include the disruption of snow as in Ferrier (1994).

*c. Graupel formation*

Graupel particles form by the interaction between supercooled drops and ice particles, its formation processes is, however, not sufficiently clarified yet. Graupel is formed when cloud ice and snow interact with supercooled droplets and supercooled rain drops collide with ice particles (cloud ice and snow). In the present study, the parameterization of graupel formation is based on the bin-like approach in the interaction of supercooled water with cloud ice and snow. In addition, an idea of "partial conversion" in each bin is introduced.

(1) Interaction between supercooled cloud droplets and cloud ice

The grauple formation by the interaction between supercooled cloud droplets and cloud ice is based on the change in bulk density and the rimed mass of supercooled water in a unit time, or riming ratio. The change in the bulk density comes from the adherence of droplets on the surface of spherical cloud ice and rimed cloud ice. In the riming process, the size distribution are divided into several bins, the riming ratio in each bin is then computed using a representative size of cloud ice in each bin. When dividing the size distribution into bins, the lower and upper bounds of the size of cloud ice are specified. The riming calculations are not made for the cloud ice whose size does not fall into between these two bounds. Very small cloud ice may not easily be transfered into graupels because of small collection efficiencies, while very large solid particles may require large amount of riming for the graupel formation.

(2) Interaction between supercooled cloud droplets and snow

The formation of graupel by the interaction between supercooled cloud droplets and snow is modeled in a similar manner as in the collision between the supercooled cloud droplets and cloud ice. For the riming process of snow, another type of riming model is taken into account in addition to the model considered for

cloud ice. Since snow has lacuna, supercooled water droplets collected in such airspace are assumed to incite the change in bulk density of snow. For this type of riming, the size of snow is unchanged during riming.

(3) Interaction of supercooled rain with cloud ice

When graupel particles form excessively from the collision between supercooled rain with cloud ice, this process is re-computed in a similar manner as the riming process of cloud ice. The size distribution of rain is sub-divided into several bins, and the collision between rain and cloud ice is considered using a representative size of cloud ice. The criteria of excessive formation of graupel is tentatively the same as in Ferrier (1994).

## 3. Preliminary results of the new model and summary

Preliminary experiments were made using JMA-NHM for a snowfall event during a cold outbreak over the Sea of Japan in order to check the performance of the new 3-ice bulk microphysical model relative to the current one. Two-moment models were employed for the solid particles of cloud ice, snow, and graupel. The model domain centered at (37.426°N, 138.887°E) was 300 km × 300 km wide in the horizontal with the grid size spacing of 1 km, and the 50 layers were considered in the vertical. The initial condition was from the meso analysis of the Japan Meteorological Agency at 12 UTC on January 16, 2011, and the lateral boundary condition was supplied from the meso analysis at three-hour intervals.

Figures 1 and 2 show surface precipitation from the new and current models, respectively. Main differences are summarized in the following two points. First, the new model ameliorates "unnatural" concentration of snowfall on the upwind slope (e.g., compare snowfall in ovals in pink in these figures). Second, the new model produced more snowfall over the Sea of Japan in wider area. It was also found that more graupels were formed in the new model (not shown).

Preliminary tests have shown that the impact of the new model is not small, and that the new model appears to have higher performance with respect to the current one.

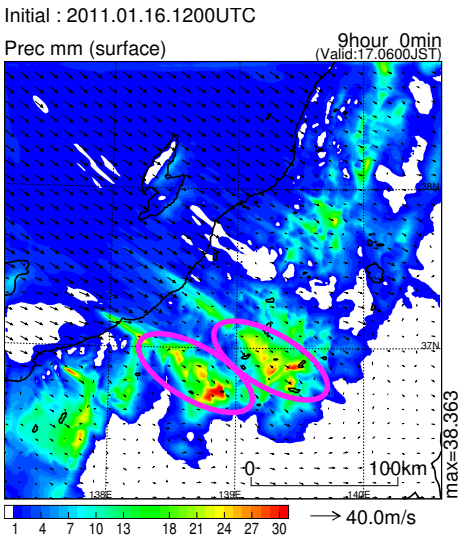


Figure 1: Hourly surface precipitation (in mm in water equivalence) between 8 and 9 forecast hours from the new model.

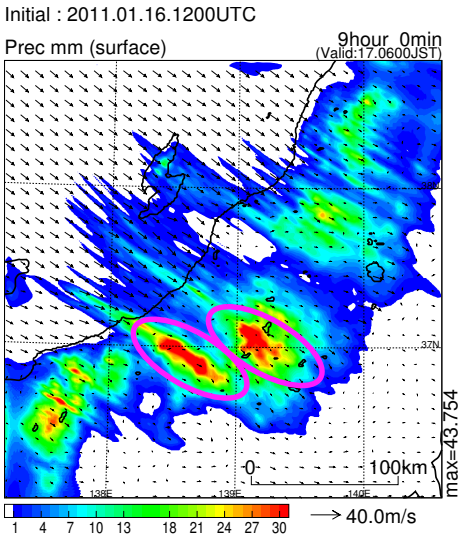


Figure 2: As in Fig. 1, except for the current model.

**Acknowledgements**

The program code of the lower incomplete Gamma function was developed in the cooperative research project concerning the photovoltaics between the Meteorological Research Institute and the Advanced Industrial Science and Technology. The development of the program code of Gauss hypergeometric function was supported by the funds for integrated promotion of social system reform, research, and development of the Ministry of Education, Culture, Sports, Science and Technology. The Gamma function code was developed referring the following web site: http://www.kurims.kyoto-u.ac.jp/ ooura/gamerf-j.html。

References

Harrington, J. Y., M. P. Meyers, R. L. Walko, and W. R. Cotton, 1995: Parameterization of ice crystal conversion processes due to vapor deposition for mesoscale models using double-moment basis functions. Part I: Basic formulation and parcel model results. *J. Atmos. Sci.*, **52**, 4344-4366.

Morrison, H. and W. W. Grabowski, 2008: A novel approach for representing ice microphysics in models: Description and tests using a kinematic framework. *J. Atmos. Sci.*, **65**, 1528-1548.

Saito, K., T. Fujita, Y. Yamada, J. Ishida, Y. Kumagai, K. Aranami, S. Ohmori, R. Nagasawa, S. Kumagai, C. Muroi, T. Kato, H. Eito, and Y. Yamazaki, 2006: The Operational JMA Nonhydrostatic Mesoscale Model. *Mon. Wea. Rev.*, **134**, 1266-1298.